Journal of Stress Analysis
Vol. 5, No. 2, Autumn − Winter 2020-21, 123-135

Bu-Ali Sina University

ORIGINAL RESEARCH PAPER

Investigation of the Notch Angle Effect on Charpy Fracture Energy in 7075-T651 Aluminum Alloy

M.R. Maraki[a], A. Hosseinzadeh[b], D. Ghahremani-Moghadam[c,*], M. Sadidi[d]

[a]Material Engineering Department, Birjand University of Technology, Birjand, Iran.
[b]Mechanical Engineering Department, Ferdowsi University of Mashhad, Mashhad, Iran.
[c]Mechanical Engineering Department, Faculty of Engineering, Quchan University of Technology.
[d]Civil Engineering Department, Shahrood University of Technology, Shahrood, Iran.

Article info

Article history:
Received 12 December 2020
Received in revised form
03 February 2021
Accepted 20 March 2021

Keywords:
Fracture energy
7075-T651 Aluminum alloy
V-shaped notch
Notch angle
Charpy impact test

Abstract

In the present study, the Charpy impact test was performed on 7075-T651 Aluminum alloy specimens with different notch angles for fracture energy measurement. In this regard, specimens with seven different notch angles were prepared, and then fracture energy was measured using the Charpy impact test. By considering the experimental results a quadratic relationship between the fracture energy (CVN in J) and the notch angle of the Charpy specimens was achieved for the tested Aluminum alloy, so the fracture energy of the 7075-T651 AA specimens was calculated for each desired notch angle. The experimental data validation was performed using mathematical modeling. Furthermore, the fracture surface of the specimens was investigated at different notch angles using SEM. By increasing the notch angle to the standard specimen, the fracture surface becomes smoother and tends to feature a brittle fracture as well as the shear lip is reduced. Moreover, for the specimens with higher notch angle (from the standard), the fracture surface tends to feature a ductile fracture and the shear lip increases.

Nomenclature

CVN	Charpy V-notch	ν	Poisson's ratio
E	Young's modulus	ρ	Notch tip radius
θ	Notch angle	σ_{rr}	Radial stress
K_I	Stress intensity factor	$\sigma_{r\theta}$	In-plane shear stress
2α	Notch opening angle	σ_u	Ultimate tensile strength
λ_i	Eigenvalues (singularity exponents)	$\sigma_{\theta\theta}$	Tangential stress
μ_i	Eigenvalues (real parameters)		

1. Introduction

Various factors are involved in empirically determining the energy of Charpy fracture. It is essential to study the variation of parameters and quantify the effective parameters on the Charpy fracture energy [1-3]. The presence of the notch causes to increase the stress concentration, which will significantly increase the stress

*Corresponding author: D. Ghahremani-Moghadam (Assistant Professor)
E-mail address: d.ghahremani@qiet.ac.ir
http://dx.doi.org/10.22084/jrstan.2021.23165.1165
ISSN: 2588-2597

applied at the crack tip [4]. The ratio of the maximum stress at the notch tip to the applied stress is called the stress concentration factor and determines the effect of notch geometry on the stress distributions at the notch tip [5]. In materials with high deformability (ductile), when the applied stress reaches a certain level, the stress concentration of the notch tip and subsequently the localized stress increase exceeds the yield stress in the front of the notch and localized plastic deformation takes place. As the maximum stress exceeds the yield stress, as the strain increases in the ductile material, the maximum stress increases slightly, the influential stress concentration factor approaches the unit value, indicating the disappearance of the notch tip [5, 6]. The brittle fracture is one of the most crucial fracture modes to be considered when securing the reliability of aluminum structures. Once it is initiated, brittle cracks can lead to the catastrophic failure of structures [7].

Druce et al. [8], using a Charpy impact test, studied the effect of notch geometry at different temperatures on SA351 CF3 steel. They investigated the U and V-notch specimens. Gomez et al. [9] used two types of U and V-notch specimens, by varying the notch depth, notch angle, and notch radius in the three-point bending experiments with PMMA polymer material. They concluded that, higher notch angle of the specimen caused higher fracture load. Ambriz et al. [10] investigated fracture energy evaluation of welded 7075-T651 Aluminum alloy using instrumented impact pendulum. In this study, fracture surfaces revealed an intergranular failure for the base metal in the longitudinal direction, whereas a predominately brittle failure (cleavage) with some insights of ductile characteristics was observed in the transverse direction. In contrast, a ductile failure was observed in the HAZ. Cova et al. [11] studied the effect of geometric size on the fracture resistance of the GJ400 iron. Hosseinzadeh and Hashemi [12] investigated the notch depth effect on Charpy fracture energy for API X65 steel experimentally. They proved a linear relationship between the notch depth and the fracture energy. Hosseinzadeh et al. [13, 14, 15] studied the notch depth, angle, and tip radius effect on Charpy fracture energy in Aluminum 7075. They extracted an exponential relationship between the notch depth and the fracture energy. Prema et al. [16] investigated characterization of corrosion and failure strength analysis of Aluminum 7075. In their study, the cast specimens were characterized by x-Ray Diffraction (XRD), Thermo Gravimetric Analysis (TGA/DSC), Energy Dispersive Spectrum (EDS), and Scanning Electron Microscope (SEM). In the case of hybrid composite, the hardness, and the tensile strength decrease when the content of Al_2O_3 increases. Hosseinzadeh et al. [17] investigated the effect of notch tip radius on fracture energy of Charpy in 7075 Aluminum alloy. Yousefzadeh et al. [18] studied the tensile and impact properties of Bagasse/Polypropylene natural composite using Charpy impact tests. Hosseinzadeh et al. [19] investigated the effect of V-notch depth on fracture toughness and the plastic zone of the crack tip using Charpy impact test data in API X65 Steel. Hosseinzadeh et al. [20] investigated the notch depth effect using instrumented impact pendulum in 7075 Aluminum alloy, and they analyzed the fracture surfaces by fractography. Hosseinzadeh and Hashemi [21] studied the notch depth effect on Charpy fracture energy in API X65 steel experimentally and numerically. Their results indicated that there was a good agreement between the experimental results and the Abaqus simulation of the Gurson model.

In the present study the effect of V-shaped notch angle variation on Charpy fracture energy was investigated, and mathematical modeling was used to validate the experimental data. Thus, the relationship between the fracture energy of 7075 Aluminum alloy and the notch angle is obtained. So in case of errors in the manufacturing of the specimens, the standard fracture energy can be calculated using the relationship that has been obtained in this study. Additionally, microstructure changes of fracture surfaces in tested specimens with different notch angles were investigated using SEM.

2. Materials and Methods

2.1. Experimental Procedure

Standard specimens were tested for Charpy impact test with geometrical specifications by ASTM E23 standard [22] with thickness, width, and length of 10, 10, and 55mm, respectively. The notch depth is also 2mm, the notch tip radius is 0.25mm, and the notch angle is 45 degrees. Fig. 1 illustrates the dimensions of a standard Charpy impact test specimen. The specimens' material is 7075-T651 Aluminum alloy. The purpose of this study is to investigate the effect of the notch angle on fracture energy. Therefore, the notch angle is considered as a variable, and the other parameters are fixed. Fig. 2 shows the specimens before fracture with different notch angles.

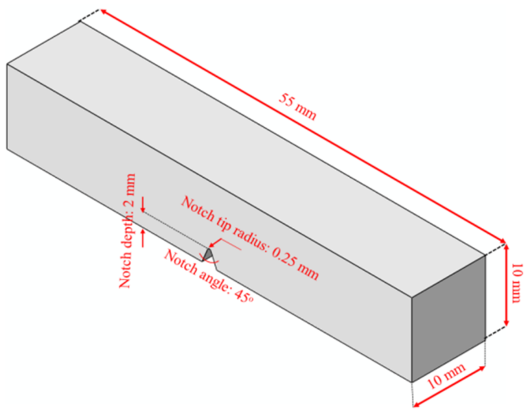

Fig. 1. Standard specimen dimensions of Charpy impact test.

Table 1
Chemical composition of 7075-T651 Aluminum alloy.

No.	1	2	3	4	5	6	7	8	9	10	11	12	13	14	15
E	Fe	Cu	Mn	Mg	Cr	Zn	Ti	Pb	V	Zr	Ag	Ga	Sb	Bi	Al
%	0.162	1.043	0.01	1.071	0.198	4.046	0.074	0.012	0.124	0.097	0.020	0.3	0.018	0.15	92.642

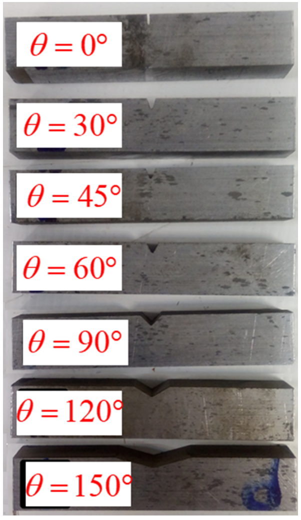

Fig. 2. The image of the specimens before fracture with different notch angles.

Table 1 gives the chemical composition of 7075-T651 Aluminum alloy measured by XRF analysis, and the mechanical properties obtained from tensile tests (Fig. 3) are presented in Table 2.

Table 2
Mechanical properties of 7075-T651 Aluminum alloy.

Mechanical properties	Value
Modulus of elasticity (GPa)	72
Yield strength (MPa)	529.78
Ultimate strength (MPa)	746.29
Poisson's ratio [23]	0.33
Micro hardness (MicroVickers)	39
Elongation%	13.2

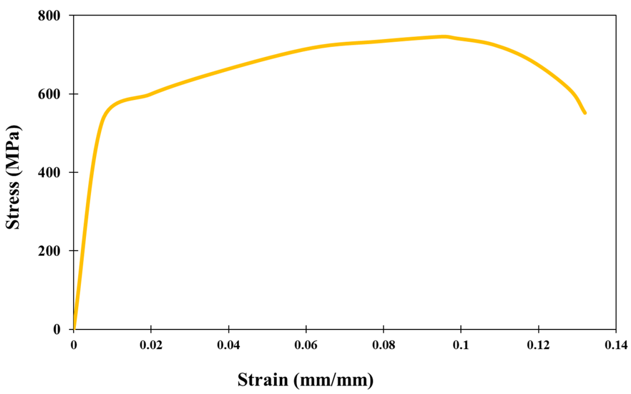

Fig. 3. Stress-strain curve for 7075 Aluminum alloy.

In this research, the notches were created on specimens using a Wire-Cut machine (electrical discharge machining). Specimens with standard dimensions of $55 \times 10 \times 10$mm and notch with the depth of 2mm and radius of 0.25mm and notch angle from 0 to 150 degrees (7 specimens with angles of 0, 30, 45, 60, 90, 120, 150 degrees) made with sufficient precision and compliance with standard requirements were used in the study.

Since the only variable parameter is the notch angle, the other parameters (notch depth, notch tip radius, etc.) should not be changed, so the dimensions (thickness, length, and width) were measured with a 50-75mm micrometer. The width and thickness were measured with a 25mm micrometer. The notch dimensions of the specimens (depth, angle, and radius) were measured with a macro lens camera and Digimizer image processing software (Fig. 4) with an accuracy of 0.001mm. In this software, each image has a resolution of 6016×4016 pixels.

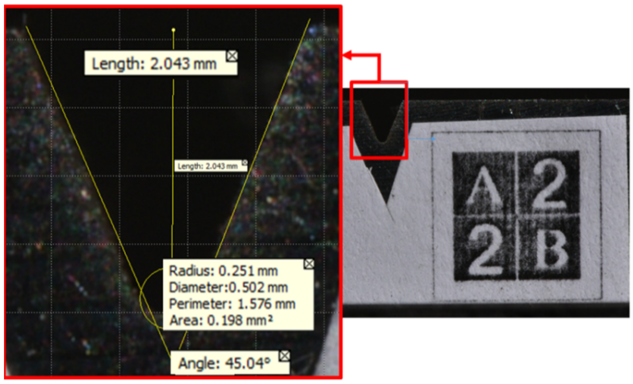

Fig. 4. Measuring specimens with digimizer software.

The impact test was performed using a Charpy Gunt impact machine with a capacity of 25J at 23°C. The Charpy impact test was repeated five times for each specimen, and the median fracture energy was obtained. This Charpy machine was equipped with an energy display system and the specimens' fracture energy could be read digitally from the monitor screen. The following images of the fracture surfaces of 7 specimens with different notch angles are shown in Fig. 5.

Charpy impact test is a destructive test procedure and in the case of the large number of test specimens, usually the strain gauge is not placed near the notch root. Furthermore, considering the dimensions of the standard thickness and width of the test specimens (5mm) and the notch depth of 2mm, there is only 3mm of space near the notch root, which is not easy to place the strain gauge near the notch root. Especially in this study where the notch angle changes and there is very little area to place the strain gauge. Therefore, in this study, such as Shterenlikht et al. [24], Hosseinzadeh et al. [20], Ali et al. [25], Kobayashi and Morita [26], Ambriz et al. [10], Vlajic et al. [27] as shown in the

Fig. 6 the strain gauge was placed on the striker.

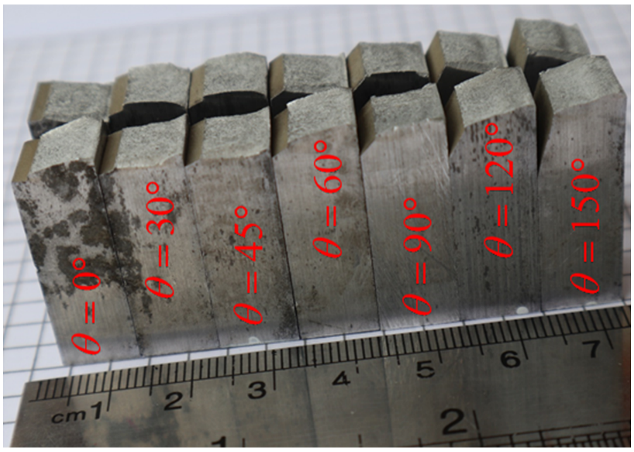

Fig. 5. The image of the specimens after fracture with different notch angles.

Charpy pendulum equipped with a strain gauge was used to evaluate the impact resistance. The strain gauges were connected to the Wheatstone bridge electrical circuit. Striker strain gauge evaluation was digitized based on ASTM E2298 using standard data acquisition system at 100kHz. Prior to impact testing, the striker was calibrated in static conditions using various loads with a hydraulic device to obtain a load-displacement assessment under elastic conditions. Strain gauges were calibrated according to ISO 14556. The load-displacement diagram was obtained from the strain gauges. Then maximum load was obtained from the load-displacement diagram. The moment of inertia where M=(F/2)×SPAN is obtained using maximum load. Then bending stress is obtained from the relationship σ=Mc/I not considering the notch. Multiply the obtained stress by the stress concentration coefficient (based on the notch geometry in the reference [28]) the maximum stress is obtained near the notch root.

2.2. Mathematical Modeling

To make usage of the notch stress intensity factors (K_I) more convenient in practical applications, the K_I are changed to the dimensionless parameters, called the notch shape factors, which depend on the specimen diameter, specimen thickness, notch depth, notch angle, and notch tip radius. Since the notch shape factors and the geometric parameters are known for a V-notch specimen, one can directly determine the values of K_I for any combination of modes I and II without requiring the FE analysis.

In the next sections, some closed-form explanations are offered in a general form for the linear elastic stress distributions around the tip of a V-shape notch under mode I loading and the K_I and notch shape factors are defined and calculated by using these expressions.

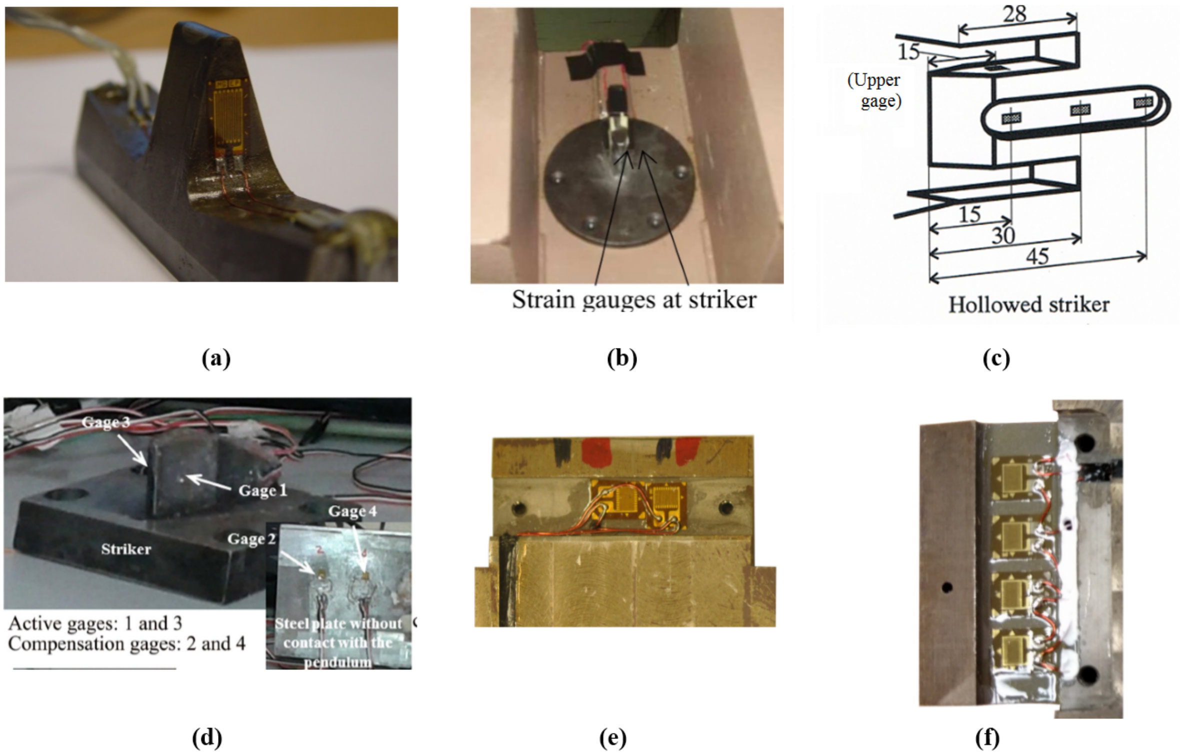

Fig. 6. The striker with attached strain gauge in some researches, a) Shterenlikht et al. [24], b) Ali et al. [25], c) Kobayashi and Morita [26], d) Ambriz et al. [10], e) and f) Vlajic et al. [27].

Figs. 7 depicts a V-shape notch in Cartesian and polar coordinate systems. Note that the coordinate origin is located on the notch bisector line and at the distance r_0 behind the notch tip to correspond the mathematical derivations of the curvilinear and Cartesian coordinate systems [29].

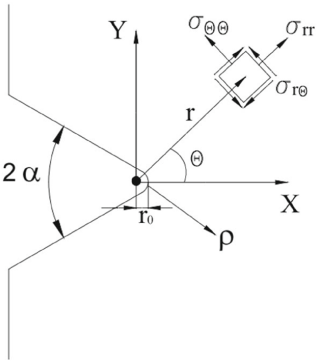

Fig. 7. A rounded-tip V-notch in Cartesian and polar coordinate system [29].

The mode I stress at the notch tip can be written as [29]:

$$\left\{\begin{array}{c}\sigma_{\theta\theta}\\ \sigma_{rr}\\ \sigma_{r\theta}\end{array}\right\}=\frac{K_I}{\sqrt{2\pi}r^{1-\lambda}}\left[\left\{\begin{array}{c}m_{\theta\theta}(\theta)\\ m_{rr}(\theta)\\ m_{r\theta}(\theta)\end{array}\right\}+\left(\frac{r}{r_0}\right)^{\mu-\lambda}\left\{\begin{array}{c}n_{\theta\theta}(\theta)\\ n_{rr}(\theta)\\ n_{r\theta}(\theta)\end{array}\right\}\right] \quad (1)$$

$\sigma_{\theta\theta}$, σ_{rr} and $\sigma_{r\theta}$ are shown in Fig. 6 and K_I is the mode I notch stress intensity factors. The functions $m_{ij}(\theta)$ and $n_{ij}(\theta)$ and also the values of the parameters $\lambda, \mu, \chi^b, \chi^c\chi^d$ for various notch angles are presented in the following.

Function $m_{ij}(\theta)$ used in the stress field for blunt V-shaped notches (mode I)) [29]:

$$\left\{\begin{array}{c}m_{\theta\theta}(\theta)\\ m_{rr}(\theta)\\ m_{r\theta}(\theta)\end{array}\right\}=\frac{1}{[1+\lambda+\chi b(1-\lambda)]}\left[\left\{\begin{array}{c}(1+\lambda)\cos(1-\lambda)\theta\\ (3-\lambda)\cos(1-\lambda)\theta\\ (1-\lambda)\sin(1-\lambda)\theta\end{array}\right\}+\chi b(1-\lambda)\left\{\begin{array}{c}\cos(1+\lambda)\theta\\ -\cos(1+\lambda)\theta\\ \sin(1+\lambda)\theta\end{array}\right\}\right] \quad (2)$$

Function $n_{ij}(\theta)$ used in the stress field for blunt V-shaped notches (mode I)) [29]:

$$\left\{\begin{array}{c}n_{\theta\theta}(\theta)\\ n_{rr}(\theta)\\ n_{r\theta}(\theta)\end{array}\right\}=\frac{1}{4(q-1)[1+\lambda+\chi b(1-\lambda)]}\left[\chi d\left\{\begin{array}{c}(1+\mu)\cos(1-\mu)\theta\\ (3-\mu)\cos(1-\mu)\theta\\ (1-\mu)\sin(1-\mu)\theta\end{array}\right\}+\chi c\left\{\begin{array}{c}\cos(1+\mu)\theta\\ -\cos(1+\mu)\theta\\ \sin(1+\mu)\theta\end{array}\right\}\right] \quad (3)$$

The values of the parameters $\lambda, \mu, \chi b, \chi c, \chi d$ for different notch angles are reported in Table 3.

Table 3
The values of the parameters $\lambda, \mu, \chi b, \chi c, \chi d$ for different notch angles [29].

2α (°)	λ	μ	χb	χc	χd
0	0.5	-0.5	1	4	0
30	0.5014	-0.4561	1.0707	3.7907	0.0632
45	0.505	-0.4319	1.1656	3.5721	0.0828
60	0.5122	0.4057	1.3123	3.2832	0.096
90	0.5448	0.3449	1.8414	2.5057	0.1046
120	0.6157	-0.2678	3.0027	1.515	0.0871
150	0.752	-0.1624	6.3617	0.5137	0.0413

According to the relationship that exists between the Cartesian and curvilinear coordinate systems, r_0 can be written as [29]:

$$r_0=\frac{q-1}{q}\rho, \qquad q=\frac{2\pi-2\alpha}{\pi} \quad (4)$$

where "2α" is the notch angle and ρ is the notch tip radius. The expressions for the notch stress intensity factor is [30]:

$$K_I=\sqrt{2\pi}\frac{(\sigma_{\theta\theta})_{\theta=0}r^{1-\lambda}}{1+w\left(\frac{r}{r_0}\right)^{\mu-\lambda}} \quad (5)$$

The expressions for the parameter ω is [29]:

$$\omega=\frac{q}{4(q-1)}\left[\frac{\chi d(1+\mu)+\chi c}{1+\lambda+\chi b(1-\lambda)}\right] \quad (6)$$

where $\sigma_{\theta\theta}$ and $\sigma_{r\theta}$ are the tangential and in-plane shear stresses, respectively. If the values of ω are known, the notch stress intensity factor can be obtained from Eq. (5) as follows [31]:

$$K_I=\sqrt{2\pi}\frac{\sigma_{\theta\theta}(r_0,0)r_0^{1-\lambda}}{1+\omega\left(\frac{r}{r_0}\right)^{\mu-\lambda}} \quad (7)$$

In the presence of the mode I stress field, it is possible to evaluate the relationship between constant a and the maximum stress at the crack tip. It can be written as [29]:

$$a = \frac{\sigma_{\max}}{\lambda r_0^{\lambda-1}\{1+\lambda+\chi b(1-\lambda)+[(1+\mu)\chi d+\chi c)]\{q/4(q-1)\}\}} \tag{8}$$

For the V-shaped notch, Gross and Mendelson [32] defined such a parameter as follows:

$$K_I = \sqrt{2\pi}\lim_{r\to 0}(\sigma_\theta)_{\theta=0} r^{1-\lambda} \tag{9}$$

From Eqs. (8) and (9), Eq. (10) can be obtained as follows:

$$K_I = \lambda\sqrt{2\pi}[1+\lambda+\chi b(1-\lambda)]a \tag{10}$$

Using Eq. (10) the relationship between the maximum stress at the tip and the notch stress intensity factor can be written as follows:

$$K_I = \sigma_{\max}\sqrt{2\pi}\left\{r_0^{1-\lambda}\Big/\left(1 + \frac{(1+\mu)\chi d+\chi c}{(1+\lambda)+\chi b(1-\lambda)}\frac{q}{4(q-1)}\right)\right\} \tag{11}$$

The maximum stress was evaluated using an instrumented impact pendulum with a strain gauge according section 2.1 explanations. The maximum stress and K_I (Eq. (11)) values are reported in Table 4.

Table 4
The values of the maximum stress and K_I.

$2\alpha(°)$	$\sigma_{\max}$ (MPa)	K_I (MPa$\sqrt{\text{mm}}$)
0	636.972	282.2509
30	653.569	272.3837
45	604.780	249.1468
60	639.384	261.6007
90	618.961	273.1329
120	529.495	291.2735
150	391.091	333.0437

Considering the Lucan relation [33] for materials with $171 < \sigma_Y < 985$MPa, Eq. (12) is obtained as follows:

$$K_I = \sqrt{\frac{E(0.53\text{CVN}^{1.28})(0.2^{0.133\text{CVN}^{0.256}})}{1000(1-\nu^2)}} \tag{12}$$

where K_I is the fracture toughness (MPa$\sqrt{\text{m}}$), CVN is the Charpy V-notch impact energy (J), σ_Y is the yield strength (MPa), E is the Young modulus (MPa), and ν is the Poisson's ratio. It can be concluded from the Eq. (12):

$$\text{CVN}^{1.28}(0.2^{0.133\text{CVN}^{0.256}}) = \frac{1000(1-\nu^2)K_I^2}{0.53E} \tag{13}$$

3. Results and Discussion

3.1. Experimental and Mathematical Modeling Results

Charpy impact tests was performed on specimens with different notch angles and the fracture energy of the specimens was measured. Fig. 8 shows the Charpy fracture energy of the specimens versus notch angle. As can be seen in Fig. 8, the specimens' fracture energy has a decreasing trend from zero-degree angle to standard size. But by increasing the angle of standard size, the fracture energy increases, indicating a large increase in the notch angle of standard sizes, the specimen behaves such as a non-notch specimen. Due to the stress concentration in the vicinity of the notches, fracture initiated from this location for all specimens. In fact by increasing the notch angle of the specimen from zero to the standard specimen, the U-shape of the zero notch angle specimen becomes V-shape for the standard notch angle specimen. So, the stress concentration increases and consequently the fracture energy decreases. According to Fig. 8, the Charpy energy can be obtained from Eq. (14) using curve fitting:

$$\text{CVN} = 0.0008\theta^2 - 0.1\theta + 12.453 \tag{14}$$

In this relation, CVN is the impact energy (J), and θ is the notch angle (degree).

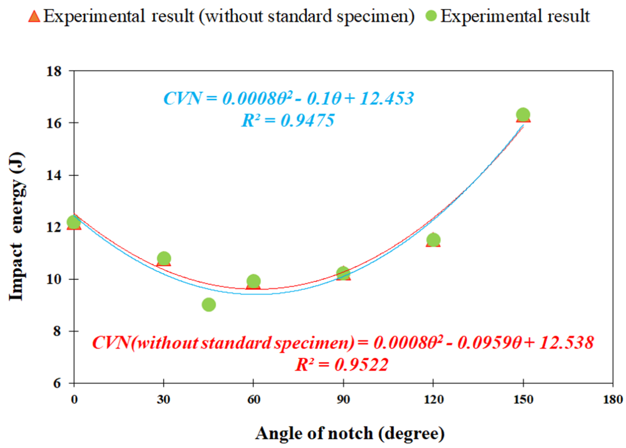

Fig. 8. Charpy fracture energy versus notch angle curve.

Two methods are employed to ensure the polynomial (Order2) relationship is obtained:

1. Remove the standard specimen from the experimental data and paste the standard specimen data into the obtained relation and determine the polynomial (Order2) relationship error percentage.

2. Based on the relation of Lucan and mathematical modeling, as the following explains.

Using Eq. (14) and by setting the standard value of the notch angle (45°), the Charpy fracture energy value is obtained 9.84J, which is in agreement with the experimental results (9.01J). One of the benefits of the obtained relationship is that by specifying the notch angle, the fracture energy of the specimen can be determined for this Aluminum alloy. Figure 8 shows the Charpy fracture energy of the specimens versus notch angle regardless of the mean fracture energy of the standard notch angle. From the Eqs. (4), (11), and (13) and Tables (1) and (3), the CVN can be obtained based on mathematical modeling. The experimental data and mathematical modeling results are shown in Fig. 9.

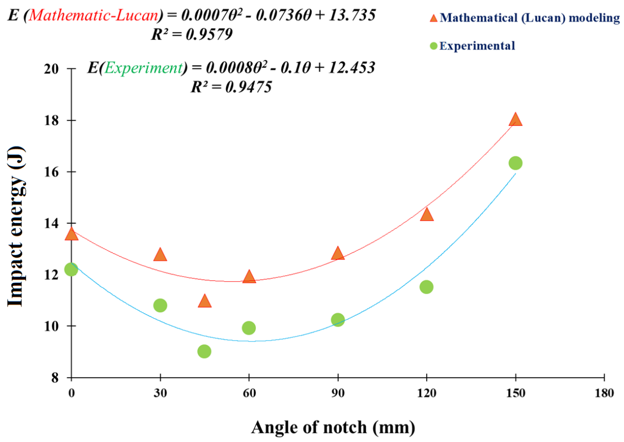

Fig. 9. Comparison of experimental and mathematical modeling results of fracture energy for different notch angles.

As can be seen in Fig. 9, both experimental data and mathematical modeling results ordered a second-order polynomial relation, which indicated the accuracy of the relationship (14). There is a slight discrepancy due to disregarding parameters such as temperature, speed, laboratory conditions, and in computing of mathematical terms.

3.2. Fractographic Observations

3.2.1. Macroscopic Morphology

Fig. 10 shows the fractured Charpy test specimens. The crack propagation of the tested specimens is in a longitudinal direction (Fig. 10) which is aligned to the expected impact load. In the transverse direction, the crack propagation describes a zigzag pattern. These characteristics were ascribed to the granular structure morphology [10].

The fracture surface of the impact specimen also comprises three regions: the fibrous region, the radial region, and the shear lip region. Fig. 11 shows the different sections of the fracture surface of the impact specimen after the Charpy impact test. The radial region, which has a smooth, grainy surface with high reflectivity and a glossy appearance, contains a cleavage indicating a brittle fracture. So by increasing the radial region proportion in the fracture surface, the fracture transition from ductile to brittle behavior can be concluded. Both the fibrous region and the shear lip region indicate a ductile fracture.

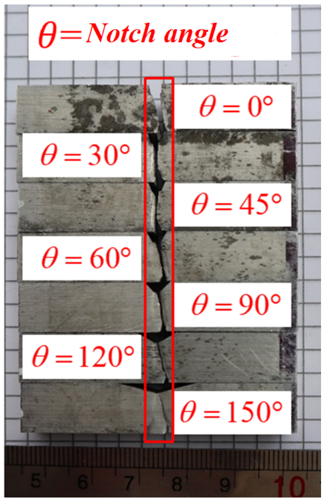

Fig. 10. Crack propagation in Charpy V-notch specimens.

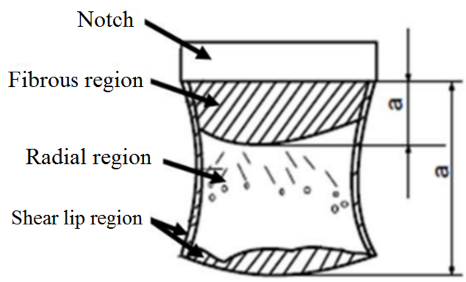

Fig. 11. The schematic fracture surface of impact specimen in macro-scale [34].

Figs. 12-13(a)-(g) shows the macroscopic photograph of the fracture surface for different notch angles. As is known, only the fibrous region and the region with shear lips can be seen at the fracture surface, and there is no radial region. The figure shows that by increasing the notch angle to the standard specimen, the fracture surface becomes smoother and tends to a brittle fracture as well as the reduction of the shear lip. Moreover, by increasing the notch angle from the standard specimen, the fracture surface is not smoothed and tends to a ductile fracture as well as the increasing of the shear lip. At the notch angle of 150°, there are cracks at the fracture surface, indicating ductile fracture. More description is in the microscopic mechanisms section.

3.2.2. Microscopic Mechanisms

Microscale ductile fracture is uniquely characterized by dimpled fracture surfaces due to microvoid coalescence. Microscale brittle fractures are characterized by either cleavage (transgranular brittle fracture) or intergranular embrittlement.

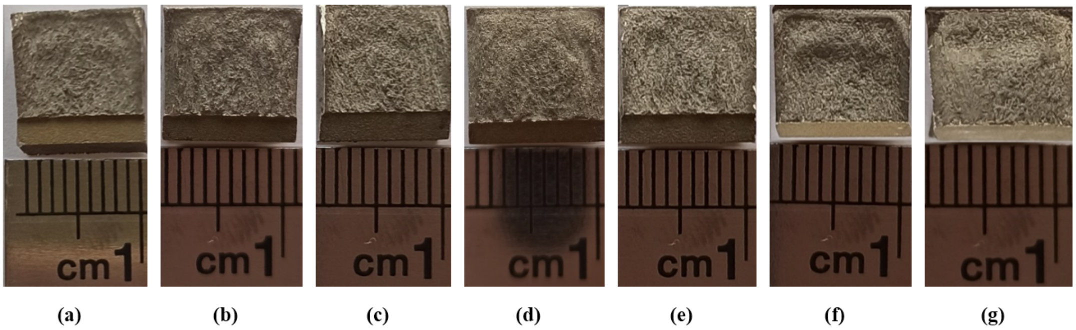

Fig. 12. Macroscopic photograph of fracture surface of impact specimens tested with different notch angle, a) 0°, b) 30°, c) 45°, d) 60°, e) 90°, f) 120°, g) 150°.

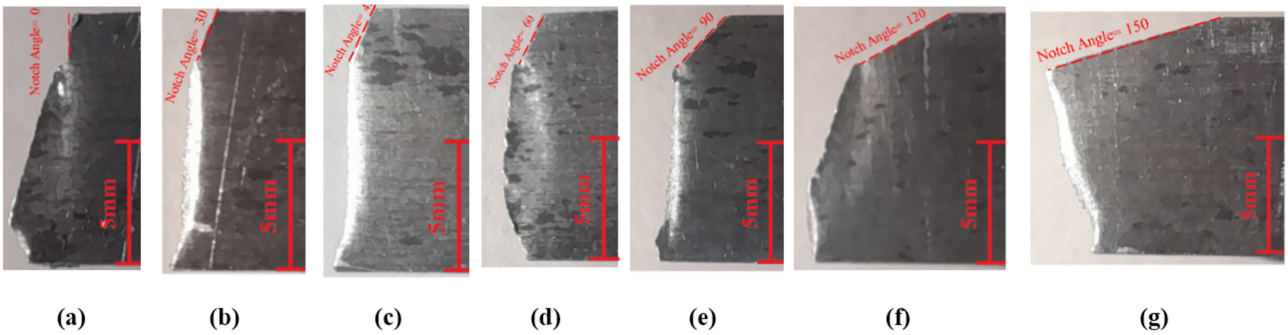

Fig. 13. Macroscopic photograph (top view) of fracture surface of impact specimens tested with different notch angle, a) 0°, b) 30°, c) 45°, d) 60°, e) 90°, f) 120°, g) 150°.

Figs. 14-20 shows the microscopic photograph of the fracture surface for different notch angles. The specimens were then placed in an ultrasonic bath for 1 hour to clear the fracture surfaces. Then, by Scanning Electron Microscopy (SEM), seven specimens whose fracture energy was close to the mean of the five repetitive specimens were depicted.

As shown in Figs. 14-20, the fracture surfaces are characterized by either cleavage or intergranular embrittlement, which is the sign of a brittle fracture.

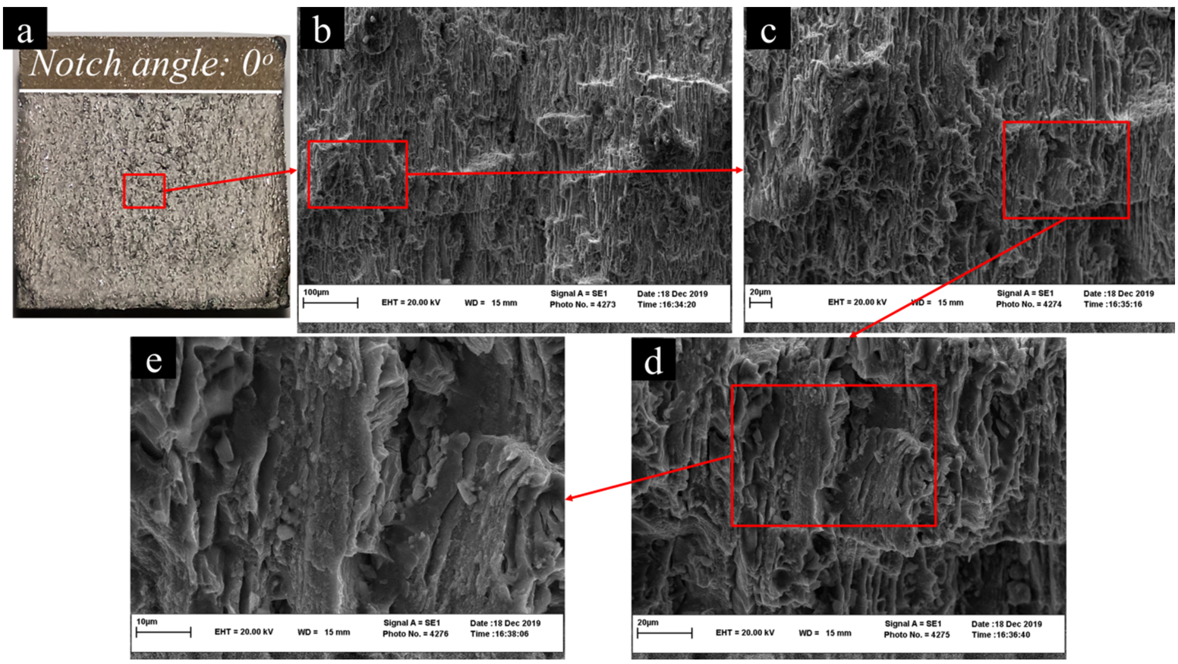

Fig. 14. Fractography of Charpy specimen with 0° notch angle with different magnifications of fracture surface.

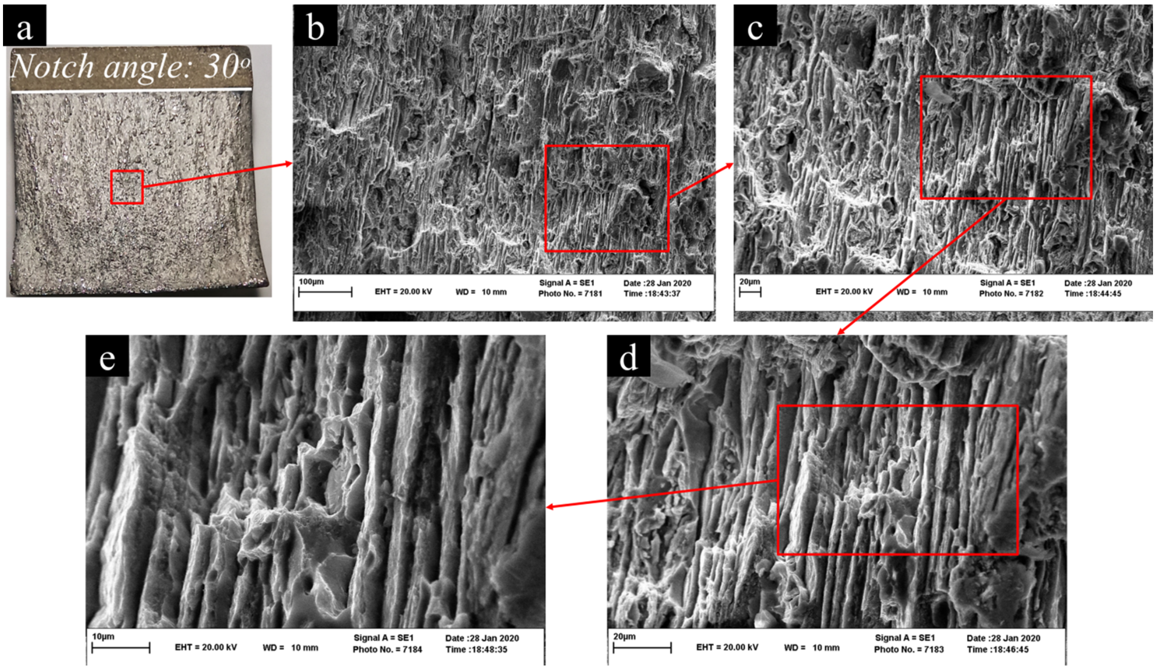

Fig. 15. Fractography of Charpy specimen with 30° notch angle with different magnifications of fracture surface.

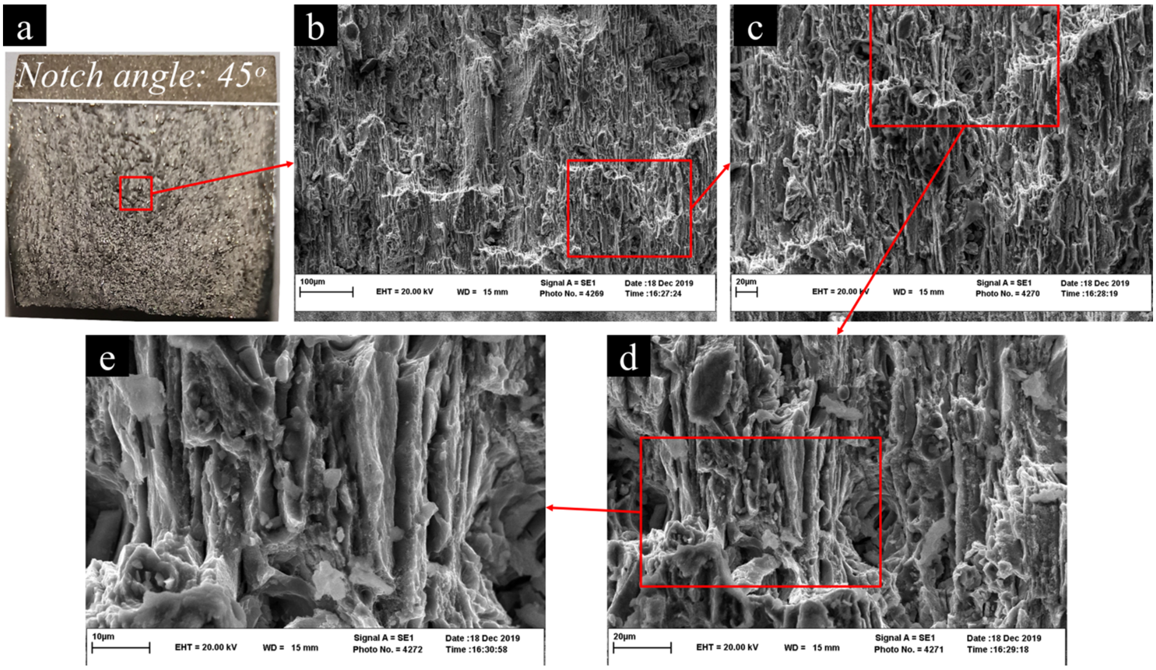

Fig. 16. Fractography of Charpy specimen with 45° notch angle with different magnifications of fracture surface.

The SEM image of the specimens depicted in four magnifications of 500x, 1000x, 2500x, and 5000x, in Figs. 14-20b, c, d, e, and f, respectively. Only the fracture surface of the specimen with the 150° notch angle in Fig. 20 has five magnifications of 100x, 500x, 1000x, 2500x, and 5000x, because there are some cracks in the fracture surface that needed more attention.

The notch angle affects the fracture energy such that at angles greater than the standard specimen (Fig. 16), the fracture energy increases, this is due to the reduction of the stress concentration at the crack tip, and crack rapid growth occurs at high angles. According to Table 3, the specimen with a notch angle of 0 degree (Fig. 14), the probability of sudden growth and directional crack is higher. But in the specimen with higher notch angles (Figs. 17-20), the notch angle has caused the deflection to move the initial crack nucleation and the stresses in the longer deflection direction to result in lower fracture speed and higher fracture energy. The pores and cracks at the fracture surface indicate that the notch angle contributes to the stress distribution in the specimen and prevents stress concentration.

The higher angle also plays a role in reducing the volume energy density because it reduces the uniformity and concentration of the stresses accumulated in front of the crack. As shown in the SEM images, the cracks and spherical cavities are more spiral and more profound at the fracture surfaces of the higher notch angle specimens. Images of cavities and cracks in the fracture surfaces show that the notch angle helps the smoother distribution of the stresses in the specimen and prevents them from accumulating.

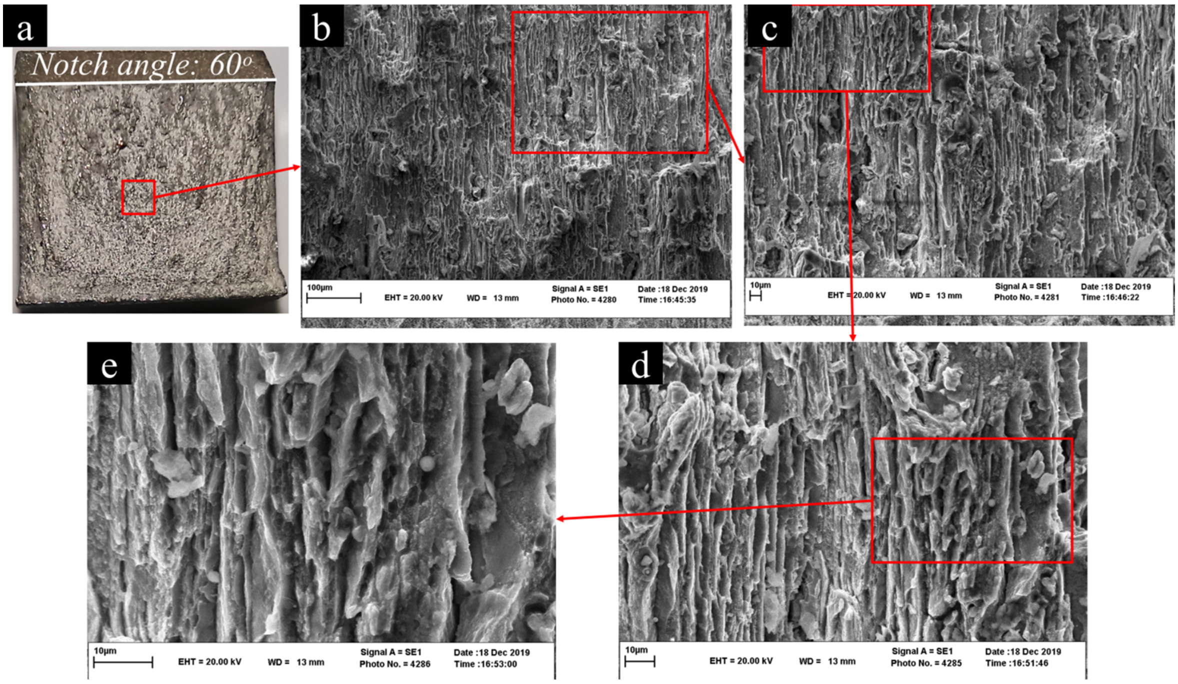

Fig. 17. Fractography of Charpy specimen with 60° notch angle with different magnifications of fracture surface.

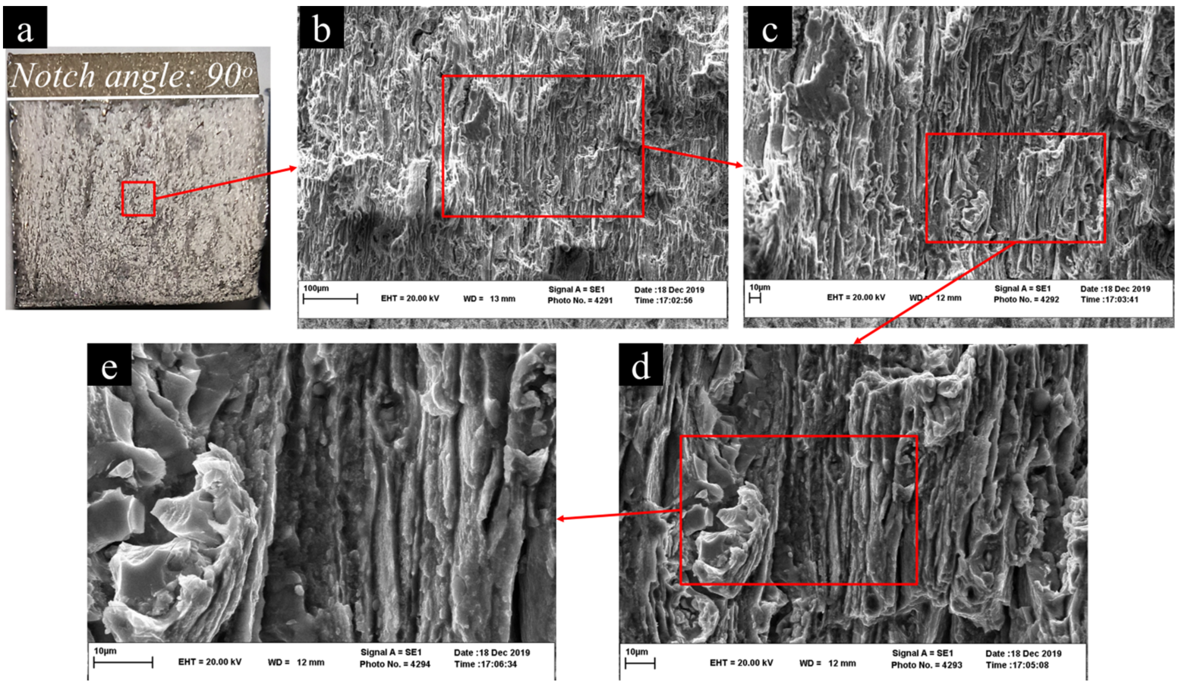

Fig. 18. Fractography of Charpy specimen with 90° notch angle with different magnifications of fracture surface.

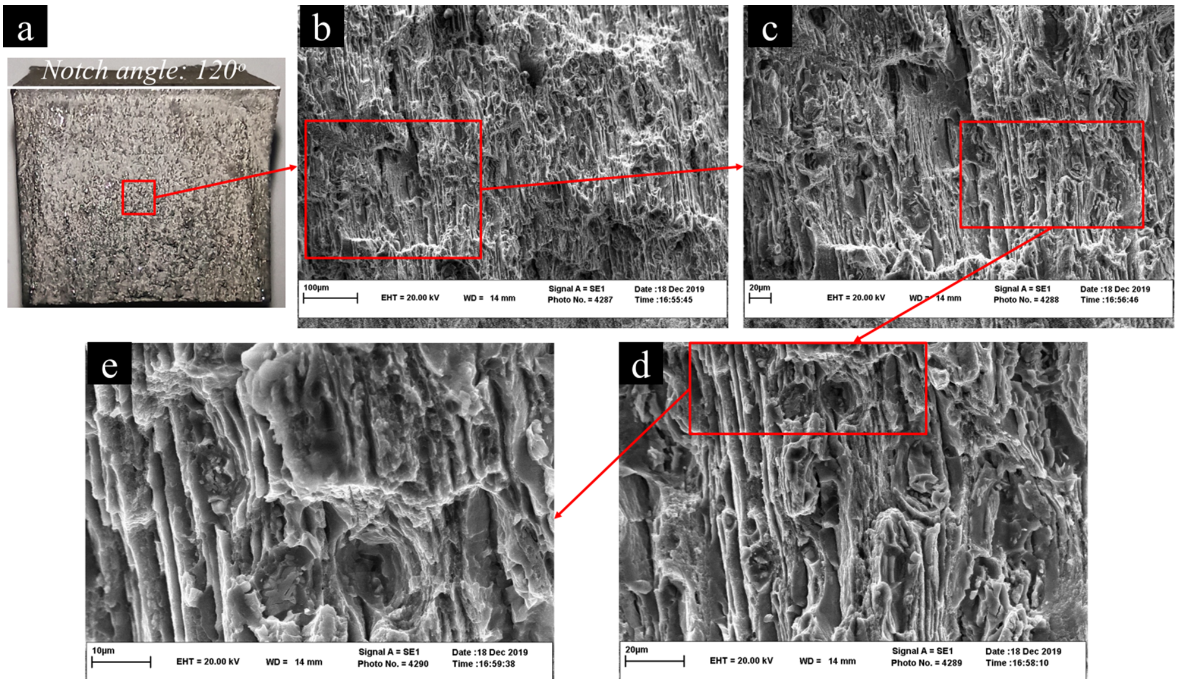

Fig. 19. Fractography of Charpy specimen with 120° notch angle with different magnifications of fracture surface.

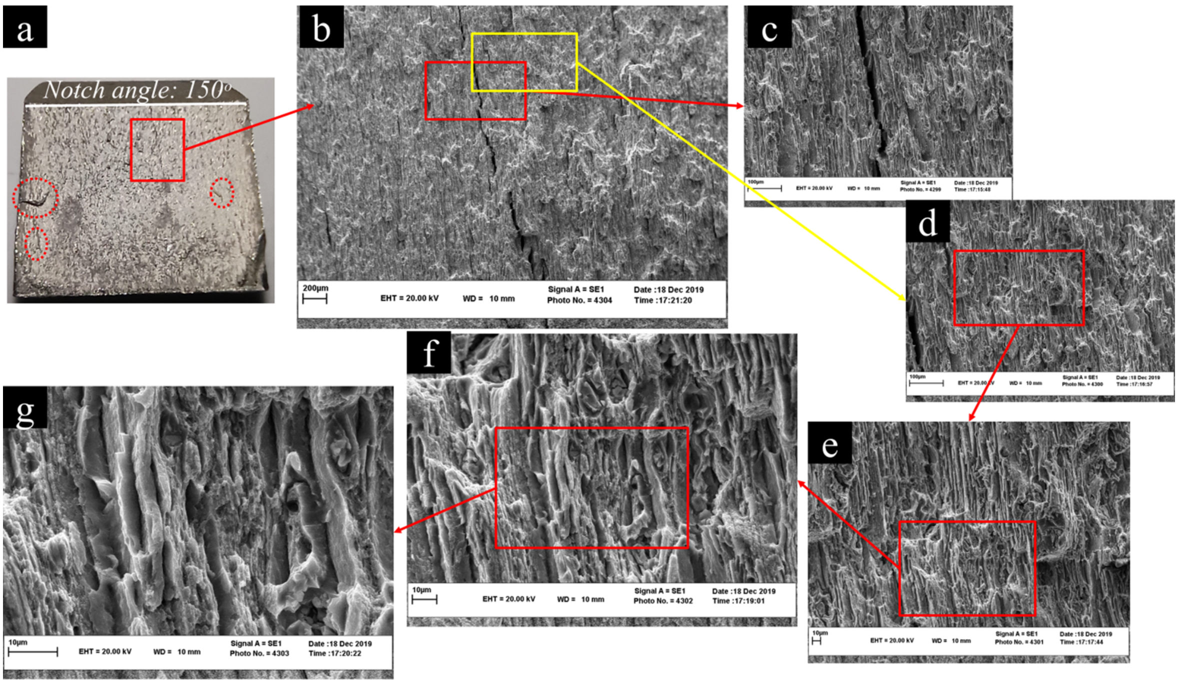

Fig. 20. Fractography of Charpy specimen with 150° notch angle with different magnifications of fracture surface.

4. Conclusions

In the present study, the effect of the notch angle on Charpy fracture energy in Aluminum 7075-T651 was investigated. Thirty-five specimens were tested in seven specimen series (each specimen was tested five times). The Charpy impact machine used in this research had the capacity of 45J, which was selected according to ASTM E23. The fracture surfaces of 7 different specimens were studied by SEM. The results are summarized as follows:

1. Using the obtained relation, the fracture energy of this Aluminum alloy can be calculated by having the value of the notch angle and placing it in the relation of $CVN = 0.0008\theta^2 - 0.1\theta + 12.453$.

2. The results showed that by increasing the notch angle to a standard size, the notch behaves such as a non-notched specimen, and the fracture energy approaches the specimen without the notch.

3. By increasing the notch angle to the standard specimen, the fracture surface becomes smoother and tends to a brittle fracture as well as the reduction of the shear lip.

4. By increasing the notch angle from the standard specimen, the fracture surface does not smooth and tends to a ductile fracture as well as the increasing of the shear lip.

Acknowledgment

The authors express their gratitude and appreciation to the Quchan University of Technology for its experimental test set up. The authors thank Mr. D. Khademi from the central laboratory of the Ferdowsi University of Mashhad.

References

[1] D. Francois, A. Pineau, From Charpy to Present Impact Testing, Elsevier Science, (2002).

[2] H. Khavanin, S.H. Hashemi, Comparison of fracture surface and charpy impact testing specimens in thermomechanical steel, Iranian Journal of Mechanical Engineers Association, 16(3) (2014) 67-78.

[3] S.H. Hashemi, Statistical analysis of charpy impact test data on grid steel pipes API X65, 4th Iranian Oil and Gas Transmission Conference, Iran, (2012).

[4] M.A. Meyers, K.K. Chawla, Mechanical Behavior of Materials, Prentice Hall, New Jersey, (1999).

[5] S.A. Sajjadi, Mechanical Behavior of Materials, Ferdowsi University of Mashhad, (2005).

[6] W.D. Pilkey, D.F. Pilkey, Peterson's Stress Concentration Factors, Third edition, John Wiley and Sons, (2007).

[7] M. Kunigita, S. Aihara, T. Kawabata, T. Kasuya, Y. Okazaki, M. Inomoto, Prediction of Charpy impact toughness of steel weld heat affected zones by combined micromechanics and stochastic fracture model, Part I: Model presentation, Eng. Fract. Mech., 230 (2020) 106965.

[8] S.G. Druce, G. Gage, E. Popkiss, Effects of notch geometry on the impact fracture behaviour of a cast duplex stainless steel, J. Pres. Ves. Piping, 33 (1988) 59-81.

[9] F.J. Gomez, M. Elices, J. Planas, The cohesive crack concept: application to PMMA at $-60°$, Eng. Fract. Mech., 72(8) (2005) 1268-1285.

[10] R.R. Ambriz, D. Jaramillo, C. Garcia, F.F. Curiel, Fracture energy evaluation on 7075-T651 aluminum alloy welds determined by instrumented impact pendulum, Trans. Nonferrous Met. Soc. China, 26(4) (2016) 974-983.

[11] M. Cova, M. Nanni, R. Tovo, Geometrical size effect in high cycle fatigue strength of heavywalled ductile cast iron GJS400: Weakest link vs defect-based approach, Procedia Eng., 74 (2014) 101-104.

[12] A. Hosseinzadeh, S.H. Hashemi, Experimental investigation of notch depth effect on Charpy fracture energy in API X65 steel, ISME2018, (2018).

[13] A. Hosseinzadeh, M.R. Maraki, A. Emamverdi, M. Sadidi, Experimental investigation of notch depth effect on Charpy fracture energy in aluminum 7075, ISME2019, (2019).

[14] A. Emamverdi, M.R. Maraki, M. Sadidi, A. Hosseinzadeh, Experimental investigation of notch tip radius effect on Charpy fracture energy in aluminum 7075, ISME2019, (2019).

[15] M.R. Maraki, M. Sadidi, A. Emamverdi, A. Hosseinzadeh, Experimental investigation of notch Angle effect on Charpy fracture energy in aluminum 7075, ISME2019, (2019).

[16] C.E. Prema, S. Suresh, G. Ramanan, M. Sivaraj, Characterization corrosion and failure strength analysis of Al7075 influenced with B4C and Nano-Al_2O_3 composite using online acoustic emission, Mater. Res. Express, 7(1) (2020) 016524.

[17] A. Hosseinzadeh, M.R. Maraki, M. Sadidi, Investigation of the effect of notch tip radius on fracture energy of Charpy in 7075 Aluminium alloy, J. Adv. Manuf. Technol., 13(2) (2020) 65-72.

[18] S. Yousefzadeh, M. Kashfi, P. Kahhal, A. Ansari-asl, An experimental investigation on tensile and impact properties of bagasse/polypropylene natural composite, AUT J. Mech. Eng., 52(8) (2020) 2149-2160.

[19] A. Hosseinzadeh, K. Farhangdoost, M.R. Maraki, Effect of V-notch depth on fracture toughness and the plastic region of the crack tip using Charpy impact test data in API X65 steel, J. Appl. Comput. Mech., 31(2) (2021) 19-32.

[20] A. Hosseinzadeh, M.R. Maraki, M. Sadidi, A. Hassani, Experimental and fractography investigation of notch depth effect by instrumented impact pendulum in 7075 Aluminum alloy, J. Solid Fluid Mech., (2021), DOI: 10.22044/jsfm.2021.9582.3172.

[21] A. Hosseinzadeh, S.H. Hashemi, Experimental investigation of notch depth effect on Charpy fracture energy in API X65 steel, ISME2018, Semnan, Iran, (2018).

[22] ASTM E23, Standard Test Methods for Notched Bar Impact Testing of Metallic Materials (Approved Nov. 10. 2002, Published May 2003).

[23] C. He, Y. Liu, J. Dong, Q. Wang, D. Wagner, C. Bathias, Fatigue crack initiation behaviors throughout friction stir welded joints in AA7075-T6 in ultrasonic fatigue, Int. J. Fatigue, 81 (2015) 171-178.

[24] A. Shterenlikht, S.H. Hashemi, J.R. Yates, I.C. Howard, R.M. Andrews, Assessment of an instrumented Charpy impact machine, Int. J. Fract., 132 (2005) 81-97.

[25] M.B. Ali, S. Abdullah, M.Z. Nuawi, A.Z. Ariffin, Investigation of energy absorbed from an instrumented Charpy impact on automotive specimens, Appl. Mech. Mater., 165 (2012) 182-186.

[26] T. Kobayashi, M. Otani, S. Morita, H. Toda, Effect of striker shape and attached position of strain gage on measured load in instrumented Charpy impact test, Proc. 4th 9nt. Sump. Impact Eng. Kumamoto, Japan, Elsevier, 86(9) (2000) 595-601.

[27] N. Vlajic, A. Chijioke, E. Lucon, Design considerations to improve Charpy instrumented strikers, Journal of Research (NIST JRES), National Institute of Standards and Technology, Gaithersburg, MD, (2020), DOI:10.6028/jres.125.010.

[28] W.D. Pilkey, D.F. Pilkey, Z. Bi, Peterson's Stress Concentration Factors, 4th Edition, John Wiley and Sons, Inc., (2020).

[29] S. Filippi, P. Lazzarin, R. Tovo, Developments of some explicit formulas useful to describe elastic stress fields ahead of notches in plates, Int. J. Solids Struct., 39(17) (2002) 4543-4565.

[30] P. Lazzarin, S. Filippi, A generalized stress intensity factor to be applied to rounded V-shaped notches, Int. J. Solids Struct., 43(9) (2006) 2461-2478.

[31] M.R. Ayatollahi, A.R. Torabi, Investigation of mixed mode brittle fracture in rounded-tip V-notched components, Eng. Fract. Mech., 77(16) (2010) 3087-3104.

[32] R. Gross, A. Mendelson, Plane elastostatic analysis of V-notched plates, Int. J. Fract. Mech., 8 (1972) 267-276.

[33] X. Li, Y. Song, Z. Ding, S. Bao, Z. Gao, A modified correlation between K_{JIC} and Charpy V-notch impact energy of Chinese SA508-III steel at the upper shelf, J. Nucl. Mater., 505 (2018) 22-29.

[34] H. Salavati, Y. Alizadeh, F. Berto, Effect of notch depth and radius on the critical fracture load of bainitic functionally graded steels under mixed mode I plus II loading, Phys. Mesomech., 17 (2014) 178-189.